

## Midlevel Ventilation's Constraint on Tropical Cyclone Intensity

BRIAN TANG AND KERRY EMANUEL

*Program in Atmospheres, Oceans, and Climate, Massachusetts Institute of Technology, Cambridge, Massachusetts*

(Manuscript received 14 September 2009, in final form 26 January 2010)

### ABSTRACT

Midlevel ventilation, or the flux of low-entropy air into the inner core of a tropical cyclone (TC), is a hypothesized mechanism by which environmental vertical wind shear can constrain a tropical cyclone's intensity. An idealized framework based on steadiness, axisymmetry, and slantwise neutrality is developed to assess how ventilation affects tropical cyclone intensity via two possible pathways: the first through downdrafts outside the eyewall and the second through eddy fluxes directly into the eyewall. For both pathways, ventilation has a detrimental effect on tropical cyclone intensity by decreasing the maximum steady-state intensity significantly below the potential intensity, imposing a minimum intensity below which a TC will unconditionally decay, and providing an upper-ventilation bound beyond which no steady tropical cyclone can exist. Ventilation also decreases the thermodynamic efficiency as the eyewall becomes less buoyant relative to the environment, which compounds the effects of ventilation alone. Finally, the formulation presented in this study is shown to be invariant across a range of thermodynamic environments after a suitable normalization and shows little sensitivity to external parameters.

### 1. Introduction

Improving forecasts of tropical cyclone (TC) intensity has proven to be a vexing challenge. Part of the challenge continues to be defining pathways by which the ambient environment controls TC intensity. One particular environmental forcing, vertical wind shear, is generally observed to be a negative factor for TC intensification and is a primary reason why the vast majority of TCs fall well short of their potential intensity (DeMaria and Kaplan 1994; Emanuel 2000; Zeng et al. 2007, 2008).

Although a causal link between vertical wind shear and TC intensity clearly exists, it is unclear how this physically comes about. Various theories have been put forth, including ventilation of the upper-level warm core (Frank and Ritchie 2001; Wong and Chan 2004), increasing tropospheric stability (DeMaria 1996), and eddy momentum fluxes (Wu and Braun 2004). The goal of this study is not to evaluate each hypothesis that has been put forth but rather to develop and analyze a simple framework for studying one hypothesis in particular:

midlevel ventilation of a TC's inner core (Simpson and Riehl 1958).

The ventilation hypothesis consists of both dynamical and thermodynamical components, and only the latter will be examined in this study. The dynamical component deals with the kinematics of how the TC vortex interacts with the environmental vertical wind shear, namely the tilt of the potential vorticity column due to differential advection by the background flow (Jones 1995; Smith et al. 2000) and the subsequent excitation of low-wavenumber asymmetries such as vortex Rossby waves (Schechter et al. 2002; Reasor et al. 2004). The thermodynamic component concentrates on how eddy fluxes of low entropy from the ambient environment by these shear-induced asymmetries subsequently interact with the tropical cyclone's energetics, thereby acting as a "constraint on the hurricane heat engine" (Simpson and Riehl 1958).

Sea surface enthalpy fluxes allow the hurricane heat engine to maintain itself against frictional dissipation, and any process that acts as a source of low-entropy air would counter the air-sea fluxes that drive the mechanical energy generation. There are two possible ways for low entropy to infiltrate the inner core, as shown in Fig. 1. The first is flushing the boundary layer with low-entropy air by convective downdrafts in the near inner-core region (Powell 1990; Riemer et al. 2009). From

---

*Corresponding author address:* Brian Tang, Massachusetts Institute of Technology, 77 Massachusetts Ave., Rm. 54-1721, Cambridge, MA 02139.  
E-mail: btangy@mit.edu

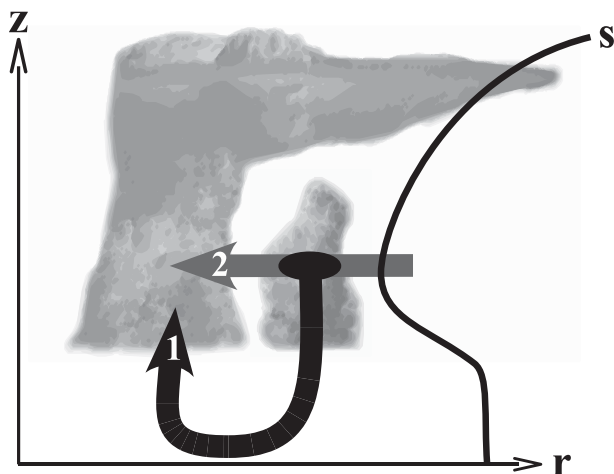


FIG. 1. Ventilation pathways by which low-entropy air can infiltrate the eyewall. (1) Low-level pathway: downdraft air from convection originating outside eyewall is advected inwards in the subcloud layer. (2) Midlevel pathway: eyewall directly ventilated by eddy fluxes. A sample entropy profile of the environmental tropical troposphere with a well-mixed subcloud layer is given on the right.

there, the low-entropy air is advected toward the eyewall by the radial inflow. We will refer to this as the “low-level pathway.” The second is direct ventilation of the eyewall, where low entropy environmental air is forced into the eyewall at midlevels by eddies (Cram et al. 2007). We will refer to this as the “midlevel pathway.” It should be recognized that in both pathways the origin of the low entropy air is always from the midlevels. Although ventilation likely operates to some degree in all TCs, given that flow asymmetries and downdrafts are commonly observed in TCs, the magnitude and scope of these negative factors in the presence of vertical wind shear may be key to how TCs respond to hostile environments. Indeed, such a response is a necessary part of the Coupled Hurricane Intensity Prediction System (CHIPS) to produce skillful intensity forecasts (Emanuel et al. 2004).

There is compelling observational evidence of ventilation occurring in reconnaissance data and that the ventilation is correlated with observed intensity changes. Reconnaissance through strongly sheared Hurricane Claudette (2003) sampled greater than  $15 \text{ m s}^{-1}$  inflow of low-entropy air at 700 hPa on the northwest side of the storm’s inner core (Shelton and Molinari 2009). Coinciding with the ventilation was a weakening of Claudette’s intensity by about  $10 \text{ m s}^{-1}$ . Additional reconnaissance data also indicated strong downdrafts spawned from precipitation falling into dry air in the inner core of sheared Hurricanes Jimena (1991) and Olivia (1994), which may have also contributed to the

weakening of both storms (Black et al. 2002). More generally, ancillary evidence of these downdrafts can commonly be seen as low-level arc clouds emanating away from sheared TCs on the upshear side.

In light of the observational and modeling evidence of ventilation, a theoretical framework is needed to assess the degree that these ventilation pathways are able to constrain a TC’s intensity. A useful starting point is the body of steady-state, axisymmetric intensity theory (Malkus and Riehl 1960; Emanuel 1986; Holland 1997; Bister and Emanuel 1998, hereafter BE98), from which one gains the benefit of a tractable framework afforded by a set of rigid assumptions, including axisymmetry, steadiness, and slantwise neutrality. Although sheared TCs are often asymmetric and unsteady in appearance, key insights in to how ventilation diminishes the symmetric component of the winds can still be garnered through this idealized approach.

A heuristic illustration of the ventilation process as a modification to the Carnot heat engine analog of a tropical cyclone is given in the first section. Section 2 then details modifications to the potential intensity theory to account for ventilation. Section 3 examines the general behavior of a ventilated tropical cyclone. In section 4, the sensitivity to various parameters is assessed, followed by concluding remarks in section 5.

## 2. Carnot engine modification

Before deriving the theoretical framework, it is useful to think about ventilation’s effect on TC intensity in a heuristic manner by considering the Carnot heat engine analog of a TC (Emanuel 1997, 2003). As shown in Fig. 2a, the secondary circulation can be divided into the four steps of the Carnot cycle, which takes the form of a rectangle on a temperature–entropy ( $T$ – $s$ ) diagram in Fig. 2b. The steps are (A) isothermal expansion in the inflow leg at the surface temperature  $T_s$ , (B) adiabatic expansion up the eyewall at a large value of moist entropy  $s_e$ , (C) isothermal compression at the outflow temperature  $T_o$ , as air radiates and subsides, and (D) adiabatic compression at an ambient value of moist entropy  $s_a$ , as air continues to subside. The area contained within the rectangle A-B-C-D in Fig. 2b is the work the cycle performs.

Now consider the effect of ventilation on this Carnot heat engine analog. Ventilating the eyewall via the midlevel pathway results in a local decrease in the entropy at midlevels along leg B. Given sufficient time, this perturbation is then spread by convective motions through a deep, slantwise layer, which is a consequence of the maintenance of subcloud layer quasi-equilibrium (Raymond 1995). As a result, the entropy decreases from  $s_e$  to  $s'_e$

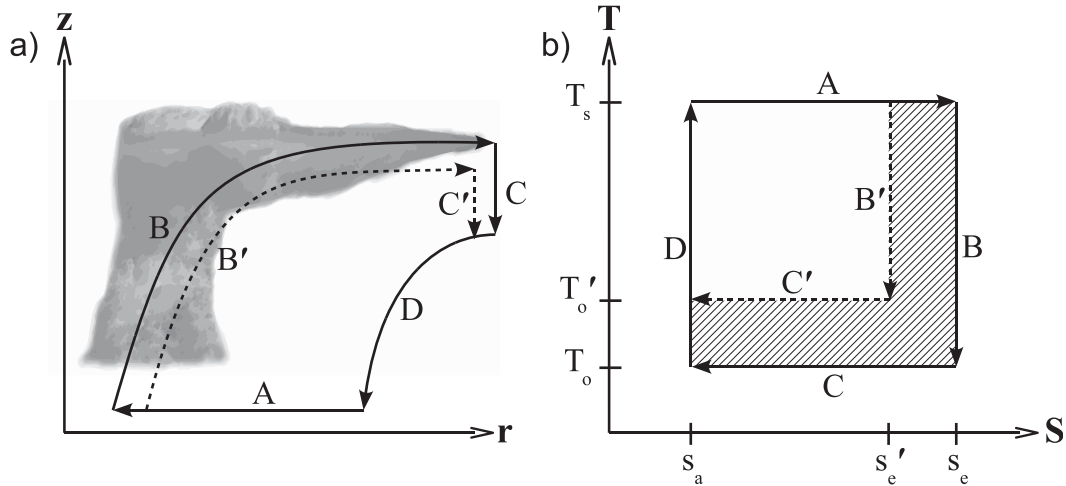


FIG. 2. (a) Secondary circulation of an idealized TC, along with (b) the legs of the secondary circulation represented on an entropy–temperature diagram. A TC without ventilation travels along A-B-C-D, whereas a ventilated TC travels along A-B'-C'-D. The hatched region in (b) denotes the work lost because of ventilation.

along leg B'. Additionally, the loss in buoyancy will correspond to a decrease in the outflow level or an increase in the outflow temperature from  $T_o$  to  $T'_o$  on leg C'. Now, consider ventilation via the low-level pathway whereby the TC boundary layer entropy is depressed by downdrafts in some region outside the eyewall. Presume that surface fluxes are unable to act to fully restore the entropy to its unperturbed value in the eyewall. Subsequently, the secondary circulation proceeds along the lower value of entropy,  $s'_e$ , in the eyewall and the outflow occurs at a higher temperature  $T'_o$ , similar to the midlevel pathway.

In both cases, the effect is detrimental to the TC heat engine. This can be plainly seen in Fig. 2b on the  $T$ - $s$  diagram as the secondary circulation of a ventilated TC follows a modified path along A-B'-C'-D, resulting in a smaller rectangle compared to the nonventilated TC. The difference in the areas of the rectangles, given by the hatched area, represents the work lost because of ventilation—work that would otherwise be used to power the winds of a TC against frictional dissipation. Ventilation thus works in two ways: it decreases the maximum difference between the ambient value of entropy and the eyewall entropy and it decreases the thermodynamic efficiency of the TC Carnot heat engine. Both of these are negative factors on TC intensity, and how much so will be examined in the next few sections.

### 3. Theoretical framework

The derivation is based on conservation principles and closely parallels that of BE98, with some major differences

that will be highlighted. Throughout the derivation, axisymmetry and steadiness are assumed. Moreover, slantwise neutrality requires that the saturation isentropes be congruent to angular momentum surfaces.

The first law of thermodynamics for saturated conditions,

$$T\delta s^* = c_p \delta T + L_v \delta q^* - \alpha \delta p, \quad (1)$$

can be combined with the momentum equations to yield

$$T\delta s^* + \frac{M}{r^2} \delta M - \frac{\alpha}{r} \zeta \delta \psi = \delta \left( E + \frac{fM}{2} \right), \quad (2)$$

where  $c_p$  is the specific heat at constant pressure,  $L_v$  is the latent heat of vaporization,  $f$  is the Coriolis parameter,  $s$  is the specific moist entropy,  $T$  is the temperature,  $q$  is the water vapor mixing ratio,  $\alpha$  is the specific volume,  $p$  is the pressure,  $M = rv + 0.5fr^2$  is the absolute angular momentum,  $\zeta$  is the azimuthal vorticity,  $\psi$  is the mass streamfunction,  $E$  is the total energy,  $r$  is the radius, and any quantity with an asterisk denotes the saturation value. The contribution of liquid water and ice to the entropy is ignored. Details on how to arrive at (2) are given in BE98.

The contribution of unbalanced flow, given by the third term in (2) containing  $\delta \psi$ , is ignored. This term is largely responsible for superintensity in numerical simulations (Bryan and Rotunno 2009) but is not critical for assessing the effects of ventilation on the potential intensity, defined by the maximum achievable gradient wind in this case.

The remaining terms are integrated around a closed circuit bounded by two isotherms and two isentropes or isopleths of angular momentum encompassing the eyewall

and adjacent region as illustrated in Fig. 3. The first and second terms on the left-hand side in (2) only have contributions from the integration along isotherms ( $T_h$  and  $\overline{T}_o$ ) while the term on the right-hand side vanishes:

$$(T_h - \overline{T}_o)\delta s^* + \int_{r_1}^{r_3} \frac{M}{r^2} \frac{\partial M}{\partial r} dr - \frac{1}{2r_o^2} \delta M^2 = 0. \quad (3)$$

To evaluate (3), expressions for  $\delta s^*$  and  $\delta M$  must be derived.

#### a. Subcloud-layer entropy

Neutrality requires  $\delta s^* = \delta s_b$ , where  $s_b$  is the subcloud-layer entropy. Hence, the entropy budget of the subcloud layer directly below the lowermost part of the integration circuit is required. In contrast to BE98, the subcloud layer is divided up in to two regions, as sketched in Fig. 4a: an “inner” region from  $r_1$  to  $r_2$  centered around the radius of maximum wind and an “outer” region from  $r_2$  to  $r_3$ . Sources and sinks of entropy in both regions include turbulent fluxes  $F_s$ , dissipative heating  $H$ , and fluxes by the mean secondary circulation. In the outer region, convective entropy fluxes,  $F_s(z = h) = \overline{w's'}$ , through the top of the subcloud layer are included. Convective downdrafts, in particular, are driven by evaporation of rain into subsaturated air supplied by eddy entropy fluxes in the free troposphere,  $\overline{\mathbf{u}'s'}$ , as will be explained in the next subsection. The division of the domain in this manner represents a generalization that can be used to study both the low-level and midlevel ventilation pathways.

In a steady state, the flux of entropy by the mean circulation through the boundaries of the subcloud-layer control volume must be equal to the sum of internal sources and sinks of entropy:

$$\int \mathbf{u}\rho s \cdot \mathbf{n} d\sigma = \int \left[ -\frac{\partial}{\partial z}(\rho F_s) + \rho H \right] dV. \quad (4)$$

To evaluate the left-hand side of (4), the definition of the mass streamfunction,

$$(u, w) = \frac{1}{\rho r} \left( -\frac{\partial \psi}{\partial z}, \frac{\partial \psi}{\partial r} \right), \quad (5)$$

is substituted, and the resulting expression is integrated by parts. Assuming  $\psi$  vanishes at the surface and  $s$  is constant with height in the subcloud layer,

$$\int \mathbf{u}\rho s \cdot \mathbf{n} d\sigma = -2\pi \int_{r_1}^{r_3} \psi \frac{\partial s}{\partial r} \Big|_h dr \approx -2\pi \overline{\psi} \delta s_b, \quad (6)$$

where  $h$  is the height of the subcloud layer. The last step in (6) approximates the integral using the average value of  $\psi$  at  $z = h$  over the radial interval.

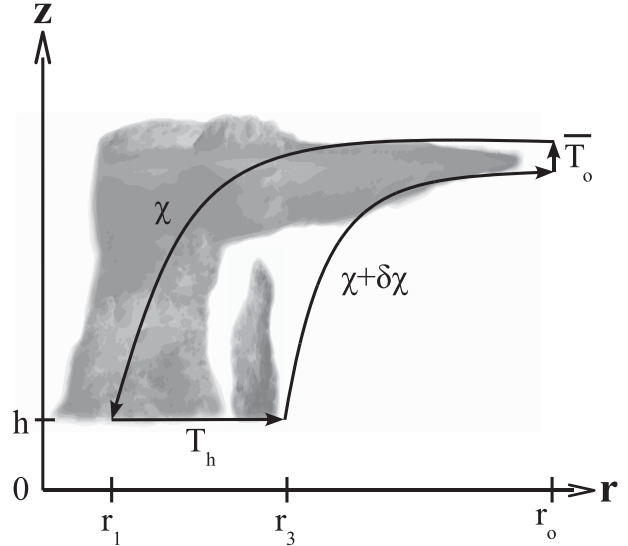


FIG. 3. Closed circuit around which (2) is evaluated. The circuit consists of two isotherms,  $T_h$  and  $\overline{T}_o$ , and two contours of constant  $\chi$ , where  $\chi \in (s^*, M, \psi)$ .

Next, the right-hand side of (4) must be evaluated separately for the inner and outer regions. The aerodynamic flux formula is used for the surface flux of entropy:

$$F_s(z=0) = C_k |\mathbf{u}| (s_{\text{SST}}^* - s_b), \quad (7)$$

along with the expression for dissipative heating from BE98:

$$\int_0^h H dz = \frac{C_D}{T_s} |\mathbf{u}|^3, \quad (8)$$

where  $C_k$  and  $C_D$  are the enthalpy and drag coefficients,  $s_{\text{SST}}^*$  is the saturation entropy at the sea surface temperature, and  $T_s$  is the surface temperature. Using (7) and (8) in the right-hand side of (4) results in

$$\begin{aligned} & \int \left[ -\frac{\partial}{\partial z}(\rho F_s) + \rho H \right] dV \\ &= 2\pi \left\{ \int_{r_1}^{r_2} \left[ \rho C_k |\mathbf{u}| (s_{\text{SST}}^* - s_b) + \frac{\rho C_D}{T_s} |\mathbf{u}|^3 \right] r dr \right. \\ & \quad \left. + \int_{r_2}^{r_3} \left[ \rho C_k |\mathbf{u}| (s_{\text{SST}}^* - s_b) + \frac{\rho C_D}{T_s} |\mathbf{u}|^3 - \rho \overline{w's'} \right] r dr \right\}. \end{aligned} \quad (9)$$

To arrive at a tractable expression, each integrand is assumed to be constant in each region. This approximation is applied by expressing  $\mathbf{u}$  as some fraction of the maximum wind velocity  $\mathbf{u}_m$  and  $r$  as some proportion of the radius of maximum wind  $r_m$  in the following fashion:

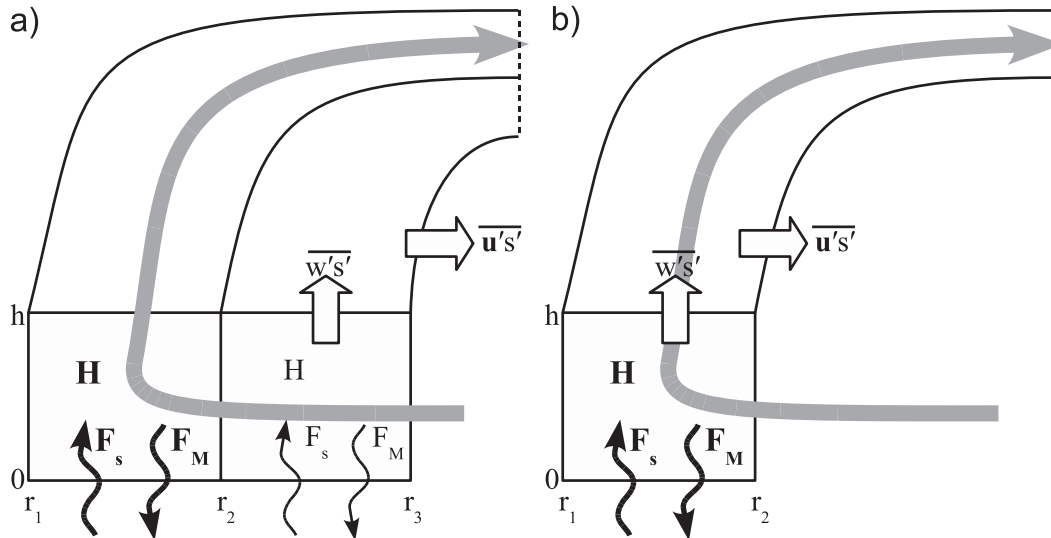


FIG. 4. Sources and sinks of entropy and angular momentum in the subcloud layer and free troposphere for the (a) low-level and (b) midlevel pathways: surface fluxes of entropy,  $F_s(z = 0)$ , and angular momentum,  $F_M(z = 0)$  (wavy arrows); dissipative heating  $H$ ; advection by the secondary circulation (gray arrow); convective entropy flux  $\overline{w's'}$  (vertical block arrow); and eddy entropy flux  $\overline{u's'}$ , through outer angular momentum surface in the free troposphere (horizontal block arrow).

$$\mathbf{u} = \begin{cases} \mathbf{u}_m & r_1 < r < r_2 \\ \gamma \mathbf{u}_m & r_2 < r < r_3 \end{cases} \quad (10)$$

$$r = \begin{cases} r_m & r_1 < r < r_2 \\ \alpha r_m & r_2 < r < r_3. \end{cases}$$

Two parameters are introduced:  $\gamma$  ( $0 \leq \gamma \leq 1$ ) controls the radial wind decay and  $\alpha$  ( $\alpha \geq 1$ ) controls the ratio of the width of both the inner and outer regions to the radius of maximum wind. Applying (10) in (9),

$$\int \left[ -\frac{\partial}{\partial z} (\rho F_s) + \rho H \right] dV \approx 2\pi r_m \delta r \left[ C_k |\mathbf{u}_m| (s_{\text{SST}}^* - s_b^i) + \frac{C_D}{T_s} |\mathbf{u}_m|^3 + C_k \alpha \gamma |\mathbf{u}_m| (s_{\text{SST}}^* - s_b^o) + \frac{C_D}{T_s} \alpha \gamma^3 |\mathbf{u}_m|^3 - \alpha \overline{w's'} \right], \quad (11)$$

where  $\delta r = r_2 - r_1 = r_3 - r_2$ ,  $s_b^i$  is the subcloud-layer entropy of the inner region, and  $s_b^o$  is the subcloud-layer entropy of the outer region. The width of both regions is chosen to be equal to simplify the analysis and should have a value that is roughly the width of a TC's eyewall.

Equating (6) and (11) yields an expression for  $\delta s_b$  or, equivalently,  $\delta s^*$ :

$$\delta s^* = -\frac{\rho r_m \delta r}{\psi} \left\{ C_k |\mathbf{u}_m| [(1 + \alpha \gamma) s_{\text{SST}}^* - (s_b^i + \alpha \gamma s_b^o)] + \frac{C_D}{T_s} (1 + \alpha \gamma^3) |\mathbf{u}_m|^3 - \alpha \overline{w's'} \right\}. \quad (12)$$

Next,  $s_b^i$  and  $s_b^o$  must be related to one another. A simple approach is to use an ‘‘upwind’’-like approximation where  $s_b^o = s_a$ , the entropy of air entering the outer region at  $r_3$ . An accurate value of  $s_a$  is ultimately needed to close the expression for the potential intensity, which requires

information about the entropy of the ambient environment along with assumptions of processes that occur along the entire inflow leg (Emanuel 1986). In this framework, an accurate value of  $s_a$  is not critical for the goal of understanding how ventilation causes differences between the steady-state intensity and potential intensity.

To get an expression for  $s_b^i$ , one must determine the entropy increase as air travels from  $r_3$  to  $r_2$ . Consider the vertically averaged entropy equation in the subcloud layer:

$$\langle u \rangle \frac{\partial s_b}{\partial r} = \frac{1}{h} \int_0^h \left( -\frac{\partial F_s}{\partial z} + H \right) dz, \quad (13)$$

where  $\langle u \rangle$  is the vertically averaged radial velocity in the subcloud layer. Using (7) and (8) and integrating from  $r_2$  to  $r_3$ ,

$$\langle u \rangle (s_b^o - s_b^i) = \frac{1}{h} \int_{r_2}^{r_3} \left[ -\overline{w's'} + C_k \gamma |\mathbf{u}| (s_{\text{SST}}^* - s_a) + \frac{C_D}{T_s} |\mathbf{u}|^3 \right] dr, \quad (14)$$

and after applying (10) and assuming the integrands are constant,  $s_b^i$  can be expressed as

$$s_b^i = s_b^o - \frac{\delta r}{\langle u \rangle h} \left[ -\overline{w's'} + C_k \gamma |\mathbf{u}_m| (s_{\text{SST}}^* - s_a) + \frac{C_D}{T_s} \gamma^3 |\mathbf{u}_m|^3 \right]. \quad (15)$$

The difference in entropy between the outer and inner regions is controlled by entropy fluxes at the top and bottom of outer region's subcloud layer, dissipative heating, the depth of the subcloud layer, and the advection time scale for parcels to travel across the outer region.

To have as few externally set parameters as possible,  $\langle u \rangle$  can be estimated by considering the vertically averaged, steady angular momentum equation:

$$\frac{1}{h} \int_0^h u \frac{\partial M}{\partial r} dz = \frac{1}{h} \int_0^h -\frac{\partial F_M}{\partial z} dz, \quad (16)$$

where  $F_M$ , the turbulent flux of angular momentum, at the surface is given by the aerodynamic flux formula:

$$F_M(z=0) = -C_D |\mathbf{u}| r v, \quad (17)$$

where  $v$  is the azimuthal velocity. Upon evaluating (16) with the assumption that  $M \approx r v$  and applying (17) followed by (10), an expression for  $\langle u \rangle$  in the outer region is obtained:

$$\langle u \rangle \approx -\frac{C_D \gamma |\mathbf{u}_m| \alpha r_m}{h}. \quad (18)$$

Substituting (18) into (15) and noting that  $\alpha \equiv 1 + \delta r/r_m$ ,

$$s_b^i = s_b^o + \Delta s = s_a + \Delta s, \\ \Delta s = \frac{\alpha - 1}{C_D \alpha \gamma |\mathbf{u}_m|} \left[ -\overline{w's'} + C_k \gamma |\mathbf{u}_m| (s_{\text{SST}}^* - s_a) + \frac{C_D}{T_s} \gamma^3 |\mathbf{u}_m|^3 \right]. \quad (19)$$

### b. Free troposphere entropy

Convective fluxes, particularly downdrafts, are a key ingredient in the subcloud-layer entropy budget in the outer region. Ventilation manifests itself through these downdrafts that are driven by the evaporation of precipitation into subsaturated air. However, it remains to

be seen how the direct effect of ventilation, namely radial eddy fluxes of entropy in the free troposphere, is connected to these convective fluxes through the top of the subcloud layer. Precisely connecting radial to convective fluxes is nontrivial as it requires treatment of microphysical processes.

However, microphysical considerations can be circumvented by applying the assumption of steadiness, which requires there be no net flux of entropy through the sides of any control volume in the absence of internal sources and sinks of entropy. Taking the control volume to be the free troposphere above the outer region (upper right region in Fig. 4a), the two prescribed fluxes that must be in balance are an inward eddy flux of low-entropy air and evaporatively cooled downdrafts at the cloud base. The latter is present if the column remains convectively active so as to maintain slantwise neutrality. If so, there is a one-to-one correspondence between these two transient fluxes:

$$2\pi \int_{r_2}^{r_3} \rho \overline{w's'} r dr = \int_{M_o} \rho \mathbf{u}' s' \cdot \mathbf{n} d\sigma. \quad (20)$$

Only radial eddy fluxes of entropy through the outer angular momentum surface  $M_o$  are considered in this case. Moreover, irreversible sources of entropy, such as that due to mixing or evaporation, have been neglected. Evaluating the left-hand side using (10) along with the constant integrand assumption and solving for  $\overline{w's'}$ ,

$$\overline{w's'} = \frac{1}{2\pi \rho \alpha r_m \delta r} \int_{M_o} \rho \mathbf{u}' s' \cdot \mathbf{n} d\sigma \equiv \mathcal{V}. \quad (21)$$

The ventilation  $\mathcal{V}$  is defined as the integrated eddy flux of entropy perpendicular to the outer angular momentum surface scaled by the downdraft area. Henceforth,  $\mathcal{V}$  is substituted where  $\overline{w's'}$  appears in (12) and (19).

### c. Subcloud-layer angular momentum

The subcloud-layer angular momentum budget proceeds similar to the entropy budget derivation. In a steady state, the flux of angular momentum through the boundaries of each subcloud-layer region must be equal to the turbulent flux of angular momentum at the surface as sketched in Fig. 4a. The fundamental equation for this balance is given by

$$\int \mathbf{u} \rho M \cdot \mathbf{n} d\sigma = \int -\frac{\partial \rho F_M}{\partial z} dV. \quad (22)$$

In the outer region, the convective flux of angular momentum is neglected in order to isolate the thermodynamic effect of ventilation, though it should be noted that

convective fluxes of angular momentum at the top of the subcloud layer are a source of superintensity (O. Pauluis and A. Mrowiec 2008, personal communication). Evaluation of (22) for each region proceeds similarly to the derivation for (12). With the use of (10) and (17),

$$\delta M = \begin{cases} \frac{r_m^2 \delta r}{\bar{\psi}} \rho C_D |\mathbf{u}_m| v_m & r_1 < r < r_2 \\ \frac{\alpha^2 r_m^2 \delta r}{\bar{\psi}} \rho C_D \gamma^2 |\mathbf{u}_m| v_m & r_2 < r < r_3. \end{cases} \quad (23)$$

Additionally,  $\bar{\psi}$  in each region is assumed to be approximately equal since the mean vertical velocity, and thus  $\partial \bar{\psi} / \partial r$ , is assumed to be small at the top of the subcloud layer in the outer region.

*d. Steady-state intensity*

All the pieces needed to evaluate the terms in (3) have now been derived. Combining (12), (19), and (21) in the first term; using (23) and assuming  $M \approx rv$  in the second term; and ignoring the third term for large  $r_o$  results in

$$\begin{aligned} & -(T_h - \bar{T}_o) \frac{\rho r_m \delta r}{\bar{\psi}} \left\{ C_k |\mathbf{u}_m| [(1 + \alpha\gamma)(s_{\text{SST}}^* - s_a) - \Delta s] \right. \\ & \left. + \frac{C_D}{T_s} (1 + \alpha\gamma^3) |\mathbf{u}_m|^3 - \alpha\mathcal{V} \right\} + \int_{r_1}^{r_2} \frac{v r_m^2}{r \bar{\psi}} \rho C_D |\mathbf{u}_m| v_m dr \\ & + \int_{r_2}^{r_3} \frac{v \alpha^2 r_m^2}{r \bar{\psi}} \rho C_D \gamma^2 |\mathbf{u}_m| v_m dr = 0. \end{aligned} \quad (24)$$

Evaluating the integrals using (10),

$$\begin{aligned} & -(T_h - \bar{T}_o) \left\{ C_k |\mathbf{u}_m| [(1 + \alpha\gamma)(s_{\text{SST}}^* - s_a) - \Delta s] \right. \\ & \left. + \frac{C_D}{T_s} (1 + \alpha\gamma^3) |\mathbf{u}_m|^3 - \alpha\mathcal{V} \right\} \\ & + C_D |\mathbf{u}_m| v_m^2 (1 + \alpha\gamma^3) = 0. \end{aligned} \quad (25)$$

The first term in the curly braces represents the energy source due to the air-sea disequilibrium with a modification factor, given by  $\Delta s$ , that increases the disequilibrium in the presence of downdrafts and decreases the disequilibrium due to entropy sources in the outer region. The second term is the recycling effect of dissipative heating, which increases the power as noted by BE98. The final term in the curly braces represents the power sink due to ventilation. The last term in (25) is the power dissipated by friction in the TC subcloud layer.

Thus far, the framework presented resembles the low-level ventilation pathway only. However, specifying  $\alpha = 1$

and  $\gamma = 0$  transforms the framework into one describing the midlevel ventilation pathway as shown in Fig. 4b. Setting  $\alpha = 1$  superposes the processes in the outer region on top of those in the inner region. Ventilation now occurs through the angular momentum surface bounding the inner region (eyewall), and convective fluxes act to redistribute entropy changes through the entire eyewall as saturation is maintained. Moreover, setting  $\gamma = 0$  is necessary to prevent a double counting of surface fluxes, dissipation, and dissipative heating in the subcloud layer. The midlevel ventilation pathway is therefore a special case of the more general framework.

As is done in BE98, it is assumed that  $T_h \approx T_s$  and  $v_m \approx |\mathbf{u}_m|$ . Upon expanding  $\Delta s$  and rearranging in to a cubic polynomial in  $|\mathbf{u}_m|$ ,

$$\begin{aligned} & \left[ \left( \frac{T_s - \bar{T}_o}{T_s} \right) \frac{C_k (\alpha - 1) \gamma^2}{\alpha} + \frac{\bar{T}_o}{T_s} C_D (1 + \alpha\gamma^3) \right] |\mathbf{u}_m|^3 \\ & + (T_s - \bar{T}_o) C_k (s_{\text{SST}}^* - s_a) \left[ -(1 + \alpha\gamma) + \frac{C_k (\alpha - 1)}{C_D \alpha} \right] |\mathbf{u}_m| \\ & + (T_s - \bar{T}_o) \left[ -\frac{C_k (\alpha - 1)}{C_D \alpha \gamma} + \alpha \right] \mathcal{V} = 0. \end{aligned} \quad (26)$$

For the trivial case where there is no ventilation ( $\mathcal{V} = 0$ ), the steady-state intensity is simply equal to the potential intensity:

$$|\mathbf{u}_{\text{PI}}^{\text{I}}|^2 = - \frac{(T_s - \bar{T}_o) C_k (s_{\text{SST}}^* - s_a) \left[ -(1 + \alpha\gamma) + \frac{C_k (\alpha - 1)}{C_D \alpha} \right]}{\left( \frac{T_s - \bar{T}_o}{T_s} \right) \frac{C_k (\alpha - 1) \gamma^2}{\alpha} + \frac{\bar{T}_o}{T_s} C_D (1 + \alpha\gamma^3)}, \quad (27)$$

which looks different from the expression in BE98. However, superposing the inner and outer regions by setting  $\alpha = 1$  and  $\gamma = 0$  collapses the current framework into that used by BE98 and results in their expression for the potential intensity:

$$|\mathbf{u}_{\text{PI}}^{\text{II}}|^2 = \frac{T_s (T_s - \bar{T}_o)}{\bar{T}_o} \frac{C_k}{C_D} (s_{\text{SST}}^* - s_a). \quad (28)$$

The difference between the potential intensities using (27) and (28) turns out to be quite small ( $<10\%$ ) for plausible combinations of  $\alpha$  and  $\gamma$ , implying that the balance between surface fluxes and dissipation solely near the radius of maximum wind is sufficient for potential intensity estimates versus needing to consider the balance over a larger region of the TC.

Using (27) or (28), two expressions for the steady-state intensity are presented when  $\mathcal{V} \neq 0$ . First, the steady-state intensity for the low-level pathway whereby the boundary

layer is flushed with low-entropy air from downdrafts outside the eyewall is

$$|\mathbf{u}_m|^3 = |\mathbf{u}_{PI}^I|^2 |\mathbf{u}_m| - \frac{(T_s - \overline{T}_o) \left[ -\frac{C_k(\alpha - 1)}{C_D \alpha \gamma} + \alpha \right]}{\left( \frac{T_s - \overline{T}_o}{T_s} \right) \frac{C_k(\alpha - 1)\gamma^2}{\alpha} + \frac{\overline{T}_o}{T_s} C_D (1 + \alpha \gamma^3)} \mathcal{V}. \quad (29)$$

Second, the steady-state intensity for the midlevel pathway whereby the eyewall is directly ventilated can be represented by letting  $\alpha = 1$  and  $\gamma \rightarrow 0$ , and (26) reduces to

$$|\mathbf{u}_m|^3 = |\mathbf{u}_{PI}^{II}|^2 |\mathbf{u}_m| - \frac{T_s(T_s - \overline{T}_o)}{\overline{T}_o} \frac{1}{C_D} \mathcal{V}. \quad (30)$$

#### 4. Behavior of a ventilated TC

Along with the heuristic picture presented in section 2, a quantitative framework for assessing midlevel ventilation's constraint on the maximum achievable steady-state intensity has been devised in the form of (29) and (30). To evaluate the behavior of both equations, it is convenient to nondimensionalize the wind speed by the potential intensity, as given by (27) or (28) depending on the pathway of interest, and the ventilation by the value of  $\mathcal{V}$  where the discriminant of the cubic polynomial vanishes:

$$\mathcal{V}_{\text{thresh}} = \frac{2}{3\sqrt{3}} \frac{|\mathbf{u}_{PI}^{\text{IorII}}|^3}{|\xi|}, \quad (31)$$

where  $\xi$  is the coefficient in front of  $\mathcal{V}$  in (29) or (30). The resulting nondimensionalization,

$$\begin{aligned} |\mathbf{u}_m| &\rightarrow |\mathbf{u}_{PI}^{\text{IorII}}| u^* \\ \mathcal{V} &\rightarrow \mathcal{V}_{\text{thresh}} \mathcal{V}^*, \end{aligned} \quad (32)$$

when substituted into either (29) or (30) results in

$$u^{*3} = u^* - \frac{2}{3\sqrt{3}} \mathcal{V}^*, \quad (33)$$

where the asterisk denotes a nondimensional variable.

Solving (33) results in up to three steady-state intensities for a ventilated TC, but only positive, real solutions are physical, which are shown in Fig. 5. The first solution branch is given by the solid line. It begins at a normalized intensity of one (the potential intensity)

and decreases monotonically as the ventilation increases, with the intensity decrease accelerating for larger values of ventilation. The second branch is given by the dashed line starting at  $0 \text{ m s}^{-1}$  and increases in intensity as the ventilation increases.

The physicality of these equilibrium solutions can be elucidated by considering the stability of each branch. Evaluating the residual of (25) as a function of  $|\mathbf{u}_m|$  and  $\mathcal{V}$  for an arbitrary set of parameters and then nondimensionalizing gives a stability diagram as depicted by the arrows in Fig. 5. Arrows pointing up indicate net energy generation and a strengthening TC while those pointing down indicate net energy dissipation and a weakening TC. Along the equilibria branches, the net energy generation must of course vanish. The arrows converge toward the first, solid solution branch, indicating that it is a stable equilibrium. Conversely, the arrows diverge from the second, dashed solution branch, indicating that it is an unstable equilibrium so that it is, in fact, an unobservable solution. Consequently, the only steady-state solution that may be observed is given by the first branch.

However, the unstable branch is useful in that it delineates intensifying and weakening regions in the  $\mathcal{V}^*$  and  $u^*$  phase space. Thus, the unstable equilibrium can be interpreted as the initial amplitude a TC needs to survive and grow in the face of ventilation. For large values of ventilation, the initial amplitude can exceed half the potential intensity.

For a normalized ventilation equal to one representing the threshold ventilation value, the steady-state intensity is reduced to 58% of the potential intensity. Beyond this, the ventilation exceeds  $\mathcal{V}_{\text{thresh}}$ , and no steady tropical cyclone can exist. Hence,  $\mathcal{V}_{\text{thresh}}$  marks the boundary between potential growth and absolute decay of a TC.

##### a. Energy budget

The monotonic decrease in intensity with increasing ventilation and threshold behavior noted in Fig. 5 can be explained further by examining the energy generation

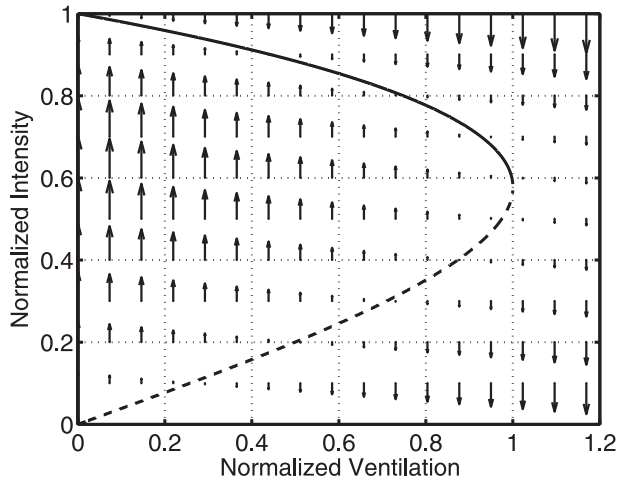


FIG. 5. Normalized equilibrium solutions (solid and dashed lines) for the steady-state intensity of a ventilated TC. Arrows denote intensifying and weakening TCs for off-equilibrium values of  $\psi^*$  and  $u^*$ .

budget within the subcloud layer as shown in Fig. 6 for the more general low-level ventilation pathway. In this calculation,  $|\mathbf{u}_{PI}| = 100 \text{ m s}^{-1}$ ,  $T_s = 28^\circ\text{C}$ ,  $\overline{T}_o = -70^\circ\text{C}$ ,  $C_k = C_D = 3 \times 10^{-3}$ ,  $\alpha = 1.5$ , and  $\gamma = 0.8$ . The power generation due to surface entropy fluxes, dissipative heating, and convective entropy fluxes [terms in curly braces in (25)] are grouped together and denoted  $G_x$  while the power loss due to frictional dissipation [final term in (25)] is denoted  $D_x$ , where  $x = i$  corresponds to the inner region and  $x = o$  to the outer region.

For low values of ventilation, convective entropy fluxes in the outer region are weak and surface fluxes dominate the budget, yielding positive power generation to balance out the frictional dissipation in both regions. As ventilation increases,  $G_o$  decreases quickly as downdrafts flush the subcloud layer with greater amounts of low entropy, leaving  $G_i$  to bear more of the burden in maintaining the TC's winds against dissipation. Once the normalized ventilation approaches one,  $G_o$  actually becomes negative as downdrafts completely overwhelm surface entropy fluxes and dissipative heating in the outer region. Now, only  $G_i$  can sustain the mechanical energy generation combating both the power dissipation due to friction and downdrafts. Ultimately, increasing the ventilation beyond the threshold level overwhelms  $G_i$ , leading to absolute decay.

A key component of  $G_i$  is the recovery of downdraft air due to the increased air-sea thermodynamic disequilibrium. Examining (29) reveals that the recovery of downdraft air reduces the effective power reduction of ventilation by a factor of  $C_k(\alpha - 1)/(C_D\alpha\gamma)$ . Increasing  $C_k$  or  $\alpha$  increases the magnitude and area over which

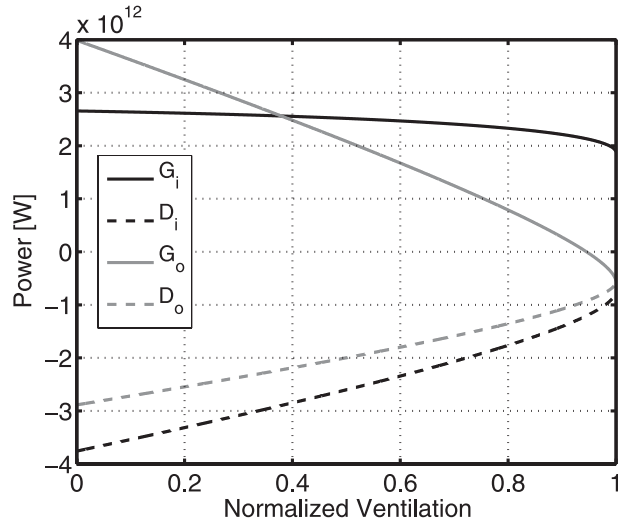


FIG. 6. Power generation and dissipation in the subcloud layer due to the combination of surface entropy fluxes, dissipative heating, and convective entropy fluxes  $G$  and friction  $D$ . Subscript  $i$  refers to the inner region and  $o$  to the outer region.

surface fluxes act to restore the downdraft modified air back to unperturbed values. On the other hand, increasing  $C_D$  or  $\gamma$  increases the frictionally driven inflow and reduces the time available for surface fluxes to act. The available recovery time is an important variable also highlighted by Powell (1990) where the short trajectories of downdraft modified boundary layer parcels in Hurricane Floyd (1981) contributed to the incomplete recovery of parcels as they spiraled in toward the radius of maximum wind.

In contrast to the low-level pathway, the midlevel pathway is more deleterious as there is no possibility of modification of the low-entropy air by surface fluxes before reaching the eyewall. One way of seeing this effect is to eliminate the recovery term in (29) by removing  $-C_k(\alpha - 1)/(C_D\alpha\gamma)$  from the numerator of the ventilation coefficient. Since this factor is negative definite, its elimination will increase the magnitude of the ventilation term. In terms of energetics, this corresponds to a more severe reduction of  $G_i$  as the power generation in the inner region must now battle both dissipation and ventilation directly, leading to more than a 40% decrease in the ventilation threshold compared to that of the low-level pathway.

*b. Midlevel pathway in Hurricane Bonnie (1998)*

Cram et al. (2007) studied Lagrangian back trajectories of parcels from an origin point in the eyewall of a numerical simulation of Hurricane Bonnie (1998), which at the time was subjected to approximately  $12 \text{ m s}^{-1}$  of

deep-layer environmental vertical shear<sup>1</sup> and had a fairly steady intensity. An estimate of the ventilation can be obtained by examining the characteristics of their “class IV,” midlevel ventilation parcels. Trajectories show that parcels had a radial velocity of approximately  $-2$  to  $-4$  m s<sup>-1</sup> while the entropy perturbations were approximately  $-10$  to  $-12$  J kg<sup>-1</sup> K<sup>-1</sup>. From their figures, it is deduced that  $r_m \approx 40$  km,  $\delta r \approx 10$  km,  $\rho \approx 1$  kg m<sup>-3</sup> at cloud base,  $\rho \approx 0.75$  kg m<sup>-3</sup> in the ventilating layer, the radius at which ventilation occurs is  $\sim 50$  km, and the depth of the ventilation layer is  $\sim 2$  km. Assuming the effect of the slope of the angular momentum surface is small, plugging all these values into (21) and setting  $\alpha = 1$  yields an estimate of the ventilation of  $3.7$ – $9$  m s<sup>-1</sup> J kg<sup>-1</sup> K<sup>-1</sup>. However, ventilation only occurs in the upshear semicircle of the storm; hence, the effective ventilation is estimated to be half this range, or between  $1.8$  and  $4.5$  m s<sup>-1</sup> J kg<sup>-1</sup> K<sup>-1</sup>.

Ideally, the next step would be to calculate a ventilation-modified steady-state intensity using (30) to compare to the simulated near-surface intensity of  $50$ – $55$  m s<sup>-1</sup>. However, this requires knowledge of the *model's* potential intensity, which is a function not only of the background thermodynamic state but also of the configuration of the model itself, including its resolution and turbulence parameterization (Rotunno et al. 2009). Using the background state only, the potential intensity in the simulation of Bonnie is estimated to range anywhere from  $27$  to  $84$  m s<sup>-1</sup> depending on the ratio of exchange coefficients and the relative humidity in the boundary layer. For instance, using the upper limit of the potential intensity range along with  $T_s = 30^\circ\text{C}$ ,  $\overline{T}_o = -63^\circ\text{C}$ , and  $C_D = 3 \times 10^{-3}$  would yield a ventilation-modified steady-state surface intensity of  $50$ – $62$  m s<sup>-1</sup>, which envelopes the simulated intensity of Bonnie. On the other hand, using the lower half of the potential intensity range would yield no steady TC as the ventilation threshold would be exceeded.

It should be emphasized that even with knowledge of the model's potential intensity, there remain a few caveats that must be highlighted. The ventilation calculation assumes that eddies and convective motions are 100% efficient at transferring the low entropy through a deep layer in the eyewall. If evaporation of rain in subsaturated air does not occur, the low-entropy air may simply enter and exit the eyewall region without much modification, leading to a reduction in the eddy entropy flux efficiency. Also, given that the standard deviation of

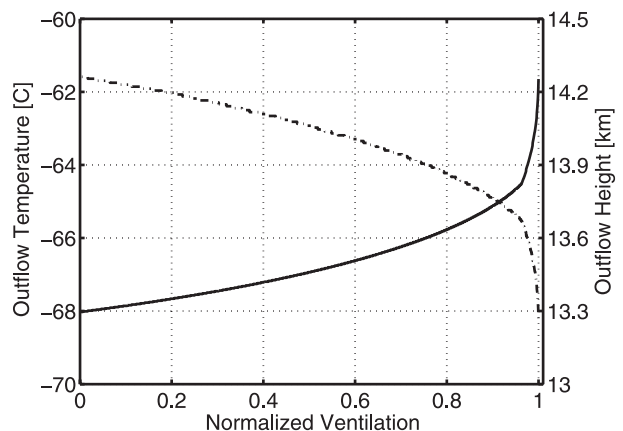


FIG. 7. Outflow temperature (solid) and height (dashed) for a ventilated TC using the Jordan hurricane season mean sounding.

the entropy perturbations is quite large in the Cram et al. (2007) study, the actual covariance between  $u'$  and  $s'$  may be significantly different from simply using the means of each to get a ballpark estimate. More precise accounting of parcels would be needed to obtain an accurate value of the ventilation.

### c. Interactive thermodynamic efficiency

In the analysis up to this point, the thermodynamic efficiency was held fixed, but ventilation acts to reduce the buoyancy of eyewall parcels relative to the environment causing the outflow temperature to increase. Such shallowing of the TC structure is supported by composited satellite derived analyses of sheared TCs (Knaff et al. 2004).

The outflow temperature is defined as the entropy-weighted temperature along surfaces of angular momentum or saturation entropy where they flare out to large radii:

$$\overline{T}_o = \frac{1}{s_{\max} - s_{\min}} \int_{s_{\min}}^{s_{\max}} T_o ds, \quad (34)$$

where  $s_{\min}$  and  $s_{\max}$  are the minimum and maximum entropy in the TC's subcloud layer. The methodology for applying (34) to a sounding is elaborated upon in the appendix.

Using the Jordan hurricane season mean sounding (Jordan 1958), the outflow temperature and height as a function of the normalized ventilation are shown in Fig. 7 for the low-level pathway. The same figure for the midlevel pathway is nearly identical. For no ventilation, the average outflow temperature is about  $-68^\circ\text{C}$ , corresponding to a thermodynamic efficiency,  $(T_s - \overline{T}_o) / \overline{T}_o$ , of 0.46. As ventilation increases, the outflow temperature warms and the outflow height lowers. As the

<sup>1</sup> The metric for vertical shear is the magnitude of the vector difference between the environmental winds at upper and lower levels of the troposphere, usually 200 and 850 hPa.

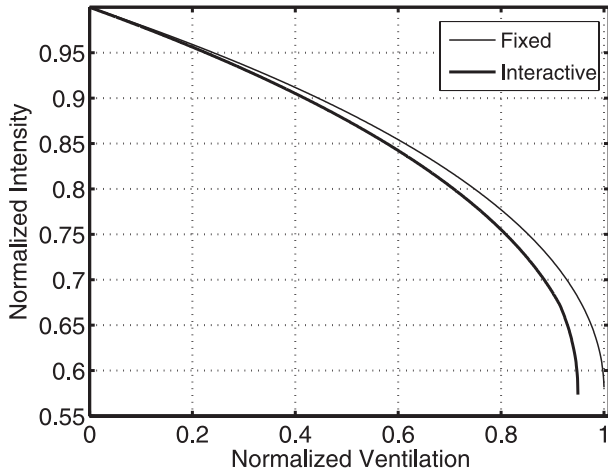


FIG. 8. Normalized steady-state intensity for fixed efficiency (thin line) and interactive efficiency (thick line).

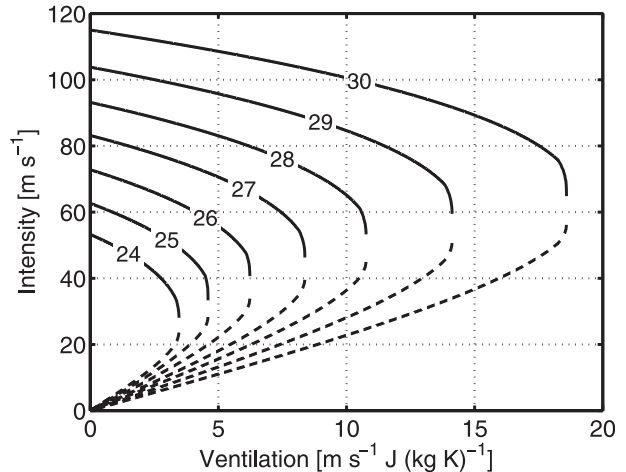


FIG. 9. Steady-state intensity curves with interactive efficiency for various thermodynamic environments binned by SST.

ventilation threshold is neared, the outflow temperature increases more rapidly as  $s_{\min}$  decreases below  $s_a$  and less buoyant parcels are included in the calculation of  $\bar{T}_o$ . Consequently, the efficiency is reduced to 0.42 at the ventilation threshold. Knaff et al. (2004) noted the height of the balanced vortex is approximately 1 km shallower in high-shear storms compared to low-shear storms, which is consistent with the change in outflow height between relatively low and high amounts of ventilation.

In comparison with fixed thermodynamic efficiency, the normalized intensity when the thermodynamic efficiency interacts with ventilation is depicted in Fig. 8. For most values of ventilation, the efficiency change contributes approximately 5%–10% to the total intensity decrease from the potential intensity, but once the ventilation becomes large, the percentage becomes much more significant. Once  $\mathcal{V}^* > 0.9$ , the contribution increases from 10% to 25% in exponential fashion.

The decreased thermodynamic efficiency is also responsible for increasing the equilibrium values along the unstable branch (not shown), which corresponds to a higher minimum intensity needed for sustainability. This change is more pronounced for larger values of ventilation. Moreover, the decrease in efficiency reduces the ventilation threshold value by a small margin over the threshold when the thermodynamic efficiency is held fixed.

### 5. Sensitivity to parameters

#### a. Potential intensity

The nondimensional form of the steady-state intensity of a ventilated tropical cyclone lacks any reference to the

potential intensity, implying that the nondimensional formulation is invariant across all background thermodynamic states. This arises because of the normalization of the ventilation by the cube of the potential intensity in (32) via (31). Differing degrees of feedback between the thermodynamic efficiency and the ventilation introduces a nominal amount of variance in the normalized intensity between thermodynamic states, especially as the ventilation approaches the threshold value, but this effect can mostly be ignored.

It is important to keep in mind that the actual ventilation can affect tropical cyclones embedded in different thermodynamic states quite differently, as shown in Fig. 9 for a range of mean tropical maritime soundings binned by sea surface temperature. The soundings are composited using 15 yr of Northern Hemisphere July–October National Centers for Environmental Prediction–National Center for Atmospheric Research (NCEP–NCAR) reanalysis data (Kalnay et al. 1996). The same value of ventilation can conceivably yield a strong TC in the more favorable thermodynamic environment and no steady TC in the other depending on whether the respective ventilation threshold has been exceeded. To observe the invariance across the environments, one must scale the intensity by the potential intensity and the ventilation by the ventilation threshold, transforming the family of curves in Fig. 9 to the single curve in Fig. 5.

#### b. Alpha and gamma

The sensitivity of the framework to the two parameters,  $\alpha$  and  $\gamma$ , is now assessed. Recall that  $\alpha$  controls the ratio of the width of the eyewall and downdraft regions to the radius of maximum wind and  $\gamma$  controls the radial

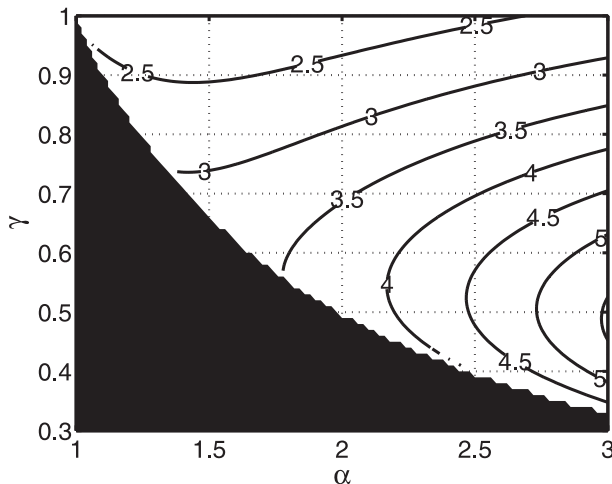


FIG. 10. Ventilation coefficient in (29) as a function of  $\alpha$  and  $\gamma$ . Values are divided by  $10^4$ . Inertially unstable combinations of  $\alpha$  and  $\gamma$  are blacked out.

decay of the wind velocity from the inner to outer regions. Given that the potential intensity only varies slightly over the plausible range of  $\alpha$  and  $\gamma$ , the sensitivity can be assessed by simply examining the coefficient in front of  $\mathcal{V}$  in (29) as a function of  $\alpha$  and  $\gamma$  while holding  $T_s = 28^\circ\text{C}$ ,  $\overline{T}_o = -70^\circ\text{C}$ , and  $C_k = C_D = 3 \times 10^{-3}$  as shown in Fig. 10. Combinations of  $\alpha$  and  $\gamma$  that yield inertially unstable configurations are blacked out.

Increasing  $\alpha$  allows a greater amount of low-entropy air to infiltrate the subcloud layer. However, increasing  $\alpha$  also allows for greater surface fluxes and recovery of downdraft air. For relatively high values of  $\gamma$ , these effects offset one another and there are only modest changes to the ventilation coefficient as  $\alpha$  varies. For smaller values of  $\gamma$ , the sensitivity of the ventilation coefficient to  $\alpha$  increases as smaller surface fluxes in the outer region are unable to promote as much recovery of downdraft air.

Over most of the parameter phase space, the ventilation coefficient is more sensitive to  $\gamma$ . As previously mentioned,  $\gamma$  controls the recovery of downdraft air with larger values of  $\gamma$  diluting the detrimental effects of downdrafts. Additionally, the frictionally induced inflow, and hence the inverse of the recovery time scale, is also directly proportional to  $\gamma$ . For relatively large  $\alpha$ , decreasing  $\gamma$  beyond a certain value results in a decrease in the ventilation coefficient as the large recovery time scale more than compensates for the small surface fluxes in the outer region.

Note that the nondimensional formulation is independent of  $\alpha$  and  $\gamma$ . Therefore, neither  $\alpha$  or  $\gamma$  affects the shape of the steady-state intensity curve in nondimensional space.

## 6. Conclusions

In the Carnot heat engine analog of a tropical cyclone, ventilation acts to reduce the maximum entropy obtained in the eyewall of the TC and reduces the thermodynamic efficiency, resulting in a decrease in the total amount of work that can be performed by the TC to combat frictional dissipation. We developed an idealized framework for analyzing the consequences of ventilation via two pathways. The first is a low-level pathway where rain evaporating into dry air aloft produces low-entropy downdrafts that are swept inwards by the radial inflow in the subcloud layer, and the second is a midlevel pathway where eddies flux low-entropy air directly into the eyewall.

Qualitatively, the behavior captured by the solutions of the analytical formulation mimics some of the gross behavioral aspects of sheared TCs. The most apparent aspect is that the maximum attainable intensity is reduced up to 58% of the potential intensity as the ventilation becomes stronger. Secondly, there is a theoretical ventilation threshold beyond which a steady tropical cyclone cannot be maintained and only a trivial solution is possible (i.e., one with no tropical cyclone at all). This is analogous to cases in which the vertical wind shear overwhelms a tropical cyclone, resulting in its quick demise, and may also explain why there are very few TCs observed for vertical wind shears greater than  $20 \text{ m s}^{-1}$  (Zeng et al. 2007, 2008). Lastly, for nonprohibitive magnitudes of ventilation, there is a dividing intensity separating growing and decaying TCs, which may be a reason why stronger and weaker storms respond differently to comparatively similar magnitudes of vertical wind shear (DeMaria et al. 2005).

The outflow temperature is affected by a shallowing of the TC's eyewall convection as its buoyancy relative to the background environment is reduced because of ventilation. This results in a reduction in the thermodynamic efficiency, which serves to compound the effects of ventilation. This is especially severe for large values of ventilation, where 10%–25% of the total weakening relative to the potential intensity can be attributed to ventilation's feedback on the thermodynamic efficiency.

TCs in environments with more favorable thermodynamic profiles (i.e., with higher potential intensities) are able to withstand ventilation better as the steady state intensity and threshold ventilation both increase while the minimum intensity needed for sustainability decreases with increasing potential intensity. Hence, the same magnitude of vertical wind shear may have quite different effects in different thermodynamic environments, allowing a fairly strong TC to be maintained in a high potential intensity environment while dissipating another TC in a low potential intensity environment.

Normalizing the steady-state intensity by the potential intensity and the ventilation by the threshold ventilation for each respective thermodynamic environment collapses the framework into a single curve that is invariant across all thermodynamic states. It would be interesting to see if, observationally, nature also follows this law. The difficulty in doing this arises in estimating the actual ventilation with observations as it would require high-density time and space observations of radial flow and entropy at midlevels in the inner core. A possible field experiment to assess these variables would involve a circular flight at midlevels just radially outside the eyewall with preferably more than one plane or combination of unmanned aerial vehicles using dropsondes to gather thermodynamic data and dual Doppler radar to assess the flow.

In the meantime, it may be possible to relate the ventilation to larger-scale, more easily observed features such as the magnitude of the vertical wind shear and internal parameters related to the TC structure, such as was done in Emanuel et al. (2004). The ventilation calculated over a larger domain from coarse gridded data, such as done in Marin et al. (2009) with the Global Forecast System model, may be sufficient for capturing some of the variance associated with ventilation-induced intensity changes. Ideally, the ventilation should be calculated as close to the inner core as possible.

A sensible approach to carry out this calculation and to test the theoretical characteristics of ventilated TCs is to use numerical simulations of ventilated or sheared TCs. An axisymmetric TC model with parameterized eddy fluxes at midlevels would be an efficient way to assess the behavior and intensity of a ventilated TC over a wide array of ventilation values and thermodynamic environments, which will be the subject of a future paper. Moreover, it would be interesting to see if the gross properties of this formulation also carry over to 3D, high-resolution simulations of sheared TCs. In particular, the connection between ventilation and resulting downdrafts needs to be examined along with the energy and entropy budgets at different annuli, specifically around the eyewall and any widespread downdrafts.

Lastly, it has been noted that changes in vertical wind shear may be an important factor in future changes in TC activity (Vecchi and Soden 2007). With an increase in potential intensity, the same amount of ventilation does comparatively less. However, as elaborated upon in Emanuel et al. (2008), the entropy deficit between the boundary layer and midlevels should increase with global warming under the assumption of constant relative humidity. Since ventilation is a function of this entropy deficit, the ventilation should correspondingly increase, leading to an increase in the entropy eddy flux

and downdraft convective available potential energy even in the event that eddy velocities are invariant with time (Nolan and Rappin 2008). Whether this corresponds to a change in the normalized ventilation, which is the relevant quantity to consider, depends largely on how the combination of vertical wind shear, entropy deficit, and potential intensity evolve with climate change.

*Acknowledgments.* We thank Mike Montgomery and Michael Riemer for their insightful discussions along with Shigeo Yoden and three anonymous reviewers for improving an earlier version of this manuscript. This work is supported by NSF Grant ATM-0850639.

## APPENDIX

### Outflow Temperature

Emanuel (1986) proposed a method for estimating the outflow temperature from a sounding by taking  $s_{\min}$  to be the ambient boundary layer entropy and  $s_{\max}$  to be the saturation entropy at the sea surface temperature. By lifting parcels with different entropies from  $s_{\min}$  to  $s_{\max}$  and calculating the temperature at their levels of neutral buoyancy, the outflow temperature  $\bar{T}_o$ , defined in (34), can be calculated.

In the ventilation framework, downdrafts can depress the subcloud-layer entropy below the ambient value, reducing  $s_{\min}$ , while the entropy difference across the inner and outer regions can be used to determine  $s_{\max}$ .

The change in entropy across both regions, given by (12), requires an expression for  $\bar{\psi}$ :

$$\psi = -\rho hr\langle u \rangle, \tag{A1}$$

and after using (18) in place of  $\langle u \rangle$  and averaging over the inner and outer regions,

$$\bar{\psi} \approx \rho C_D |\mathbf{u}_m| r_m^2 \left( \frac{1 + \alpha^2 \gamma}{2} \right). \tag{A2}$$

Using (A2) and the identity  $\delta r/r_m = \alpha - 1$ , (12) becomes

$$\delta s = -\frac{2(\alpha - 1)}{C_D |\mathbf{u}_m| (1 + \alpha^2 \gamma)} \left\{ C_k |\mathbf{u}_m| [(1 + \alpha \gamma)(s_{\text{ST}}^* - s_a) - \Delta s] + \frac{C_D}{T_s} (1 + \alpha \gamma^3) |\mathbf{u}_m|^3 - \alpha \overline{w' s'} \right\}. \tag{A3}$$

Given a sounding and sea surface temperature, Eq. (A3) must be applied in an iterative manner as follows. As a first guess,  $s_{\min}$  is set to the average entropy of the lowest 100 hPa of the sounding and  $s_{\max}$  is set to  $s_{\text{ST}}^*$ .

Then an estimate of the outflow temperature can be calculated using (34), where  $T_o$  is the temperature at the level of neutral buoyancy. With the outflow temperature estimate, the steady-state intensity is evaluated using (29), which can then be used to assess the entropy change across the outer region using (19) and the entire region using (A3). If (19) is negative, then  $s_{\min}$  is adjusted down to reflect the fact that downdrafts have lowered the entropy below  $s_a$ . Otherwise,  $s_{\min}$  is unchanged. Likewise, (A3) is used to adjust  $s_{\max}$ , which should be greater than  $s_a$ . A new outflow temperature is calculated and the entire procedure is repeated until convergence occurs, usually in a few iterations.

A drawback of this method is that as  $\alpha$  approaches 1, the entropy jump vanishes as the radial region over which fluxes act approaches a delta function. This precludes the ability of the algorithm to estimate the outflow temperature correctly and leads to an underestimate of the thermodynamic efficiency. It is recommended that  $\alpha \geq 1.5$  when calculating the outflow temperature in order to avoid this deficiency.

#### REFERENCES

- Bister, M., and K. Emanuel, 1998: Dissipative heating and hurricane intensity. *Meteor. Atmos. Phys.*, **65**, 233–240.
- Black, M., J. Gamache, F. Marks, C. Samsury, and H. Willoughby, 2002: Eastern Pacific Hurricanes Jimena of 1991 and Olivia of 1994: The effect of vertical shear on structure and intensity. *Mon. Wea. Rev.*, **130**, 2291–2312.
- Bryan, G., and R. Rotunno, 2009: Evaluation of an analytical model for the maximum intensity of tropical cyclones. *J. Atmos. Sci.*, **66**, 3042–3060.
- Cram, T., J. Persing, M. Montgomery, and S. Braun, 2007: A Lagrangian trajectory view on transport and mixing processes between the eye, eyewall, and environment using a high-resolution simulation of Hurricane Bonnie (1998). *J. Atmos. Sci.*, **64**, 1835–1856.
- DeMaria, M., 1996: The effect of vertical shear on tropical cyclone intensity change. *J. Atmos. Sci.*, **53**, 2076–2087.
- , and J. Kaplan, 1994: Sea surface temperature and the maximum intensity of Atlantic tropical cyclones. *J. Climate*, **7**, 1324–1334.
- , M. Mainelli, L. Shay, J. Knaff, and J. Kaplan, 2005: Further improvements to the Statistical Hurricane Intensity Prediction Scheme (SHIPS). *Wea. Forecasting*, **20**, 531–543.
- Emanuel, K., 1986: An air–sea interaction theory for tropical cyclones. Part I: Steady-state maintenance. *J. Atmos. Sci.*, **43**, 585–604.
- , 1997: Some aspects of hurricane inner-core dynamics and energetics. *J. Atmos. Sci.*, **54**, 1014–1026.
- , 2000: A statistical analysis of tropical cyclone intensity. *Mon. Wea. Rev.*, **128**, 1139–1152.
- , 2003: Tropical cyclones. *Annu. Rev. Earth Planet. Sci.*, **31**, 75–104.
- , C. DesAutels, C. Holloway, and R. Korty, 2004: Environmental control of tropical cyclone intensity. *J. Atmos. Sci.*, **61**, 843–858.
- , R. Sundararajan, and J. Williams, 2008: Hurricanes and global warming: Results from downscaling IPCC AR4 simulations. *Bull. Amer. Meteor. Soc.*, **89**, 347–367.
- Frank, W., and E. Ritchie, 2001: Effects of vertical wind shear on the intensity and structure of numerically simulated hurricanes. *Mon. Wea. Rev.*, **129**, 2249–2269.
- Holland, G., 1997: The maximum potential intensity of tropical cyclones. *J. Atmos. Sci.*, **54**, 2519–2541.
- Jones, S., 1995: The evolution of vortices in vertical shear. I: Initially barotropic vortices. *Quart. J. Roy. Meteor. Soc.*, **121**, 821–851.
- Jordan, C., 1958: Mean soundings for the West Indies area. *J. Meteor.*, **15**, 91–97.
- Kalnay, E., and Coauthors, 1996: The NCEP/NCAR 40-Year Reanalysis Project. *Bull. Amer. Meteor. Soc.*, **77**, 437–471.
- Knaff, J., S. Seseske, M. DeMaria, and J. Demuth, 2004: On the influences of vertical wind shear on symmetric tropical cyclone structure derived from AMSU. *Mon. Wea. Rev.*, **132**, 2503–2510.
- Malkus, J., and H. Riehl, 1960: On the dynamics and energy transformations in steady-state hurricanes. *Tellus*, **12**, 1–20.
- Marin, J., D. Raymond, and G. Raga, 2009: Intensification of tropical cyclones in the GFS model. *Atmos. Chem. Phys.*, **9**, 1407–1417.
- Nolan, D., and E. Rappin, 2008: Increased sensitivity of tropical cyclogenesis to wind shear in higher SST environments. *Geophys. Res. Lett.*, **35**, L14805, doi:10.1029/2008GL034147.
- Powell, M., 1990: Boundary layer structure and dynamics in outer hurricane rainbands. Part II: Downdraft modification and mixed layer recovery. *Mon. Wea. Rev.*, **118**, 918–938.
- Raymond, D., 1995: Regulation of moist convection over the West Pacific warm pool. *J. Atmos. Sci.*, **52**, 3945–3959.
- Reasor, P., M. Montgomery, and L. Grasso, 2004: A new look at the problem of tropical cyclones in vertical shear flow: Vortex resiliency. *J. Atmos. Sci.*, **61**, 3–22.
- Riemer, M., M. Montgomery, and M. Nicholls, 2009: A new paradigm for intensity modification of tropical cyclones: Thermodynamic impact of vertical wind shear on the inflow layer. *Atmos. Chem. Phys. Discuss.*, **9**, 10 711–10 775.
- Rotunno, R., Y. Chen, W. Wang, C. Davis, J. Dudhia, and G. Holland, 2009: Large-eddy simulation of an idealized tropical cyclone. *Bull. Amer. Meteor. Soc.*, **90**, 1783–1788.
- Schechter, D., M. Montgomery, and P. Reasor, 2002: A theory for the vertical alignment of a quasigeostrophic vortex. *J. Atmos. Sci.*, **59**, 150–168.
- Shelton, K., and J. Molinari, 2009: Life of a six-hour hurricane. *Mon. Wea. Rev.*, **137**, 51–67.
- Simpson, R., and R. Riehl, 1958: Mid-tropospheric ventilation as a constraint on hurricane development and maintenance. Preprints, *Tech. Conf. on Hurricanes*, Miami Beach, FL, Amer. Meteor. Soc., D4-1–D4-10.
- Smith, R., W. Ulrich, and G. Sneddon, 2000: On the dynamics of hurricane-like vortices in vertical-shear flows. *Quart. J. Roy. Meteor. Soc.*, **126**, 2653–2670.
- Vecchi, G., and B. Soden, 2007: Increased tropical Atlantic wind shear in model projections of global warming. *Geophys. Res. Lett.*, **34**, L08702, doi:10.1029/2006GL028905.
- Wong, M., and J. Chan, 2004: Tropical cyclone intensity in vertical wind shear. *J. Atmos. Sci.*, **61**, 1859–1876.
- Wu, L., and S. Braun, 2004: Effects of environmentally induced asymmetries on hurricane intensity: A numerical study. *J. Atmos. Sci.*, **61**, 3065–3081.
- Zeng, Z., Y. Wang, and C. Wu, 2007: Environmental dynamical control of tropical cyclone intensity—An observational study. *Mon. Wea. Rev.*, **135**, 38–59.
- , L. Chen, and Y. Wang, 2008: An observational study of environmental dynamical control of tropical cyclone intensity in the Atlantic. *Mon. Wea. Rev.*, **136**, 3307–3322.